of CMG2 (PDB ID code 1SHT)[11] was manually placed in the electron density. Model building was performed with O[25] and TURBOFRODO (A. Roussel and C. Cambillau, Silicon Graphics), and the solvent structure was built with ARP/wARP 6.0 (ref. 26). Although the random errors in the diffraction data are high, owing to the small crystal size, the final refinement statistics and maps are excellent (Table 1). Thus, the final *R*-factors are $R_{free} = 26.6\%$ and $R_{work} = 20.7\%$ overall, and $R_{free} = 37.2\%$ and $R_{work} = 27.5\%$ in the outer resolution bin, with root-mean-square deviations (r.m.s.d.) from ideal values of 0.017 Å for bond lengths and 1.65° for angles. Stereochemistry is excellent as assessed with PROCHECK[24], and the model is consistent with composite simulated annealing omit maps (3,000 °C) calculated in CNS[27]. The model comprises residues 16–735 of PA; 41–210 of CMG2, with the exception of three loops (residues 159–174, 276–287 and 304–319) in PA for which no electron density was observed; 139 water molecules; two Ca^{2+} ions in PA domain I; two Na^{+} ions; one PEG molecule; and one Mn^{2+} ion at the MIDAS site. The *B* factors for the Ca^{2+} and Mn^{2+} ions (27–33 $Å^2$) are higher than for the coordinating residues (16–20 $Å^2$). Although the MIDAS metal ion *in vivo* is likely to be Mg^{2+}, we have previously shown for integrin I domains that the stereochemistry of the open conformation is not dependent on the nature of the metal ion[5]. The bond lengths to the Mn^{2+} ion are 2.1 ± 0.2 Å, identical to those observed in integrin–ligand complexes[5,13,28]. PA domain I (residues 16–258) undergoes a small rotation as a consequence of crystal constraints when compared with the structure of isolated PA such that the r.m.s.d. values for the superposition of the two molecules are 1.44, 0.58 and 0.79 Å for residues 16–735, 259–735 and 16–258 respectively. CMG2 residues 41–200 superimpose with a r.m.s.d. of 0.60 with the isolated protein[11], while the C-terminal helix (residues 201–210) shifts downwards by one helical turn.

Received 6 May; accepted 18 June 2004; doi:10.1038/nature02763.
Published online 4 July 2004.

1. Moayeri, M. & Leppla, S. H. The roles of anthrax toxin in pathogenesis. *Curr. Opin. Microbiol.* **7,** 19–24 (2004).
2. Abrami, L., Liu, S., Cosson, P., Leppla, S. H. & Vander Goot, F. G. Anthrax toxin triggers endocytosis of its receptor via a lipid raft-mediated clathrin-dependent process. *J. Cell Biol.* **160,** 321–328 (2003).
3. Bradley, K. A., Mogridge, J., Mourez, M., Collier, R. J. & Young, J. A. Identification of the cellular receptor for anthrax toxin. *Nature* **414,** 225–229 (2001).
4. Scobie, H. M., Rainey, G. J., Bradley, K. A. & Young, J. A. Human capillary morphogenesis protein 2 functions as an anthrax toxin receptor. *Proc. Natl Acad. Sci. USA* **100,** 5170–5174 (2003).
5. Emsley, J., Knight, C. G., Farndale, R. W., Barnes, M. J. & Liddington, R. C. Structural basis of collagen recognition by integrin α2β1. *Cell* **101,** 47–56 (2000).
6. Petosa, C., Collier, R. J., Klimpel, K. R., Leppla, S. H. & Liddington, R. C. Crystal structure of the anthrax toxin protective antigen. *Nature* **385,** 833–838 (1997).
7. Benson, E. L., Huynh, P. D., Finkelstein, A. & Collier, R. J. Identification of residues lining the anthrax protective antigen channel. *Biochemistry* **37,** 3941–3948 (1998).
8. Nassi, S., Collier, R. J. & Finkelstein, A. PA63 channel of anthrax toxin: an extended β-barrel. *Biochemistry* **41,** 1445–1450 (2002).
9. Frankel, A. E., Koo, H.-K., Leppla, S. H., Duesbury, N. S. & Vande Woude, G. F. Novel protein targeted therapy of metastatic melanoma. *Curr. Pharm. Des.* **9,** 2060–2066 (2003).
10. Lee, J.-O., Rieu, P., Arnaout, M. A. & Liddington, R. C. Crystal structure of the A-domain from the α subunit of integrin CR3 (CD11b/CD18). *Cell* **80,** 631–635 (1995).
11. Lacy, D. B., Wigelsworth, D. J., Scobie, H. M., Young, J. A. & Collier, R. J. Crystal structure of the von Willebrand factor A domain of human capillary morphogenesis protein 2: An anthrax toxin receptor. *Proc. Natl Acad. Sci. USA* **101,** 6367–6372 (2004).
12. Wigelsworth, D. J. *et al.* Binding stoichiometry and kinetics of the interaction of a human anthrax toxin receptor, CMG2, with protective antigen. *J. Biol. Chem.* **279,** 23349–23356 (2004).
13. Shimaoka, M. *et al.* Structures of the αL I domain and its complex with ICAM-1 reveal a shape-shifting pathway for integrin regulation. *Cell* **112,** 99–111 (2003).
14. Rosovitz, M. J. *et al.* Alanine scanning mutations in domain 4 of anthrax toxin protective antigen reveal residues important for binding to the cellular receptor and to a neutralizing monoclonal antibody. *J. Biol. Chem.* **278,** 30936–30944 (2003).
15. Bradley, K. A. *et al.* Binding of anthrax toxin to its receptor is similar to α integrin-ligand interactions. *J. Biol. Chem.* **278,** 49342–49347 (2003).
16. Mourez, M. *et al.* Mapping dominant-negative mutations of anthrax protective antigen by scanning mutagenesis. *Proc. Natl Acad. Sci. USA* **100,** 13803–13808 (2003).
17. Miller, C. J., Elliott, J. L. & Collier, R. J. Anthrax protective antigen: prepore-to-pore conversion. *Biochemistry* **38,** 10432–10441 (1999).
18. Petosa, C. in *Crystal Structure of the Anthrax Protective Antigen*. Thesis, Harvard Univ (1995).
19. Song, L. *et al.* Structure of staphylococcal alpha-hemolysin, a heptameric transmembrane pore. *Science* **274,** 1859–1866 (1996).
20. Nanda, A. & St Croix, B. Tumor endothelial markers: new targets for cancer therapy. *Curr. Opin. Oncol.* **16,** 44–49 (2004).
21. Nanda, A. *et al.* TEM8 interacts with the cleaved C5 domain of collagen alpha 3(VI). *Cancer Res.* **64,** 817–820 (2004).
22. Liu, S., Schubert, R. L., Bugge, T. H. & Leppla, S. H. Anthrax toxin: structures, functions and tumour targeting. *Expert Opin. Biol. Ther.* **3,** 843–853 (2003).
23. Otwinowski, Z. & Minor, W. Processing of X-ray diffraction data collected in oscillation mode. *Methods Enzymol.* **276,** 307–326 (1997).
24. Collaborative Computational Project, No. 4. The CCP4 suite: programs for protein crystallography. *Acta Crystallogr. D* **50,** 760–763 (1994).
25. Jones, T. A., Zou, J.-Y., Cowan, S. W. & Kjelgaard, M. Improved methods for building protein models into electron density maps and the location of errors in these models. *Acta Crystallogr. A* **47,** 110–119 (1991).
26. Morris, R. J., Perrakis, A. & Lamzin, V. S. ARP/wARP and automatic interpretation of protein electron density maps. *Methods Enzymol.* **374,** 229–244 (2003).
27. Brunger, A. T. *et al.* Crystallography & NMR system: A new software suite for macromolecular structure determination. *Acta Crystallogr. D* **54,** 905–921 (1998).
28. Lee, J.-O., Bankston, L. A., Arnaout, M. A. & Liddington, R. C. Two conformations of the integrin A-domain (I-domain): a pathway for activation? *Structure* **3,** 1333–1340 (1995).
29. Sanner, M. F., Olson, A. J. & Spehner, J. C. Reduced surface: an efficient way to compute molecular surfaces. *Biopolymers* **38,** 305–320 (1996).

Acknowledgements We thank the NIH and the DOD for financial support, and the DOE and staff at the SSRL for synchrotron access and support.

Competing interests statement The authors declare that they have no competing financial interests.

Correspondence and requests for materials should be addressed to R.C.L. (rlidding@burnham.org). The atomic coordinates have been deposited in the Protein Data Bank under accession code 1T6B.

Cell cycle regulation of central spindle assembly

Masanori Mishima[1], Visnja Pavicic[1], Ulrike Grüneberg[2], Erich A. Nigg[2] & Michael Glotzer[1]

[1]*Research Institute of Molecular Pathology, Dr. Bohrgasse 7, A-1030 Vienna, Austria*
[2]*Max-Planck-Institute für Biochemie, Am Klopferspitz 18a, D-82152 Martinsried, Germany*

The bipolar mitotic spindle is responsible for segregating sister chromatids at anaphase. Microtubule motor proteins generate spindle bipolarity and enable the spindle to perform mechanical work[1]. A major change in spindle architecture occurs at anaphase onset when central spindle assembly begins. This structure regulates the initiation of cytokinesis and is essential for its completion[2]. Central spindle assembly requires the centralspindlin complex composed of the *Caenorhabditis elegans* ZEN-4 (mammalian orthologue MKLP1) kinesin-like protein and the Rho family GAP CYK-4 (MgcRacGAP). Here we describe a regulatory mechanism that controls the timing of central spindle assembly. The mitotic kinase Cdk1/cyclin B phosphorylates the motor domain of ZEN-4 on a conserved site within a basic amino-terminal extension characteristic of the MKLP1 subfamily. Phosphorylation by Cdk1 diminishes the motor activity of ZEN-4 by reducing its affinity for microtubules. Preventing Cdk1 phosphorylation of ZEN-4/MKLP1 causes enhanced metaphase spindle localization and defects in chromosome segregation. Thus, phosphoregulation of the motor domain of MKLP1 kinesin ensures that central spindle assembly occurs at the appropriate time in the cell cycle and maintains genomic stability.

At the metaphase–anaphase transition, the anaphase-promoting complex triggers proteolysis of cyclin B (an activating subunit of the mitotic kinase Cdk1) and sister chromatid separation. Chromosomes move polewards and non-kinetochore spindle microtubules become bundled, initiating assembly of the central spindle, a structure that has important roles in cytokinesis. In *C. elegans* embryos and other animal cells, central spindle assembly requires centralspindlin[3]. Many proteins that regulate mitosis and cytokinesis re-localize upon anaphase onset. For example, Aurora B and its associated subunits dissociate from centromeres and concentrate on the central spindle[4–6]. Similarly, anaphase onset triggers redistribution of centralspindlin (Fig. 1a, b). In metaphase, centralspindlin is diffuse and in anaphase it localizes to the microtubules positioned between the separating chromosomes, as seen previously[7–10]. ZEN-4 (also known as CeMKLP1) colocalizes with the proline-directed phosphatase CDC-14 (ref. 11) and depletion of CDC-14 prevents ZEN-4 localization[12]. Non-degradable cyclins stabilize Cdk1 activity and prevent central spindle assembly[13,14]. Together these data

indicate that ZEN-4 localization is controlled, directly or indirectly, by a proline-directed kinase-phosphatase switch. However, it is not yet known in molecular detail how ZEN-4 localization is controlled and whether this regulatory pathway has important biological implications.

As a first step in evaluating how centralspindlin localization is regulated, we assessed whether the motor domain of ZEN-4 (amino acids 1–434; referred to hereafter as ZEN-4^{MOT}) is a substrate for Cdk1/cyclin B *in vitro*. ZEN-4 and its orthologues contain an N-terminal Cdk1 consensus site (S/T)-P-X-(K/R) that is conserved among most animal species (Fig. 1c). ZEN-4^{MOT} was efficiently phosphorylated by Cdk1/cyclin B. In contrast, a protein variant in which the conserved phosphoacceptor site was substituted by alanine (ZEN-4$^{MOT\text{-}T9A}$) was not phosphorylated (Fig. 1d). The motor domain of the mammalian orthologue of ZEN-4, MKLP1, was also phosphorylated by Cdk1/cyclin B on the corresponding site, T8, and one additional site, T450 (Fig. 1e). The phosphorylation site in ZEN-4, T9, is located in a ~20-residue extension N-terminal to the catalytic core that is found in the MKLP1 subfamily and in some, but not all, kinesin-like proteins. In the MKLP1 subfamily this extension is highly basic; phosphorylation at this site would reduce the overall charge on this extension.

MKLP1 and its orthologues have not previously been shown to support microtubule motility in standard gliding assays. However, lysates from bacteria expressing MKLP1 have been shown to support antiparallel microtubule gliding at 0.07 $\mu m\,s^{-1}$ (ref. 15). Therefore, we adapted the conventional gliding assay, using purified ZEN-4 motor domain biotinylated at its carboxy terminus to facilitate oriented adsorption to a glass surface[16]. ZEN-4^{MOT} supported robust microtubule motility *in vitro* over a range of ionic conditions (25–250 mM KCl), at an average velocity of 0.16 $\mu m\,s^{-1}$ (Supplementary Movie 1). ZEN-4 constructs that contain the entire neck region translocated microtubules more rapidly (average velocity 0.4 $\mu m\,s^{-1}$) (unpublished results, M.M. and M.G.). We note that microtubule gliding does not require the ZEN-4 binding partner CYK-4.

To assess the function of the N-terminal extension that contains the Cdk1/cyclin B phosphorylation site, we compared the ATPase activity and motility of ZEN-4^{MOT} with ZEN-4$^{\Delta N}$ (amino acids 21–434). Under physiological salt conditions (150 mM KCl), the microtubule-activated ATPase activity of ZEN-4$^{\Delta N}$ is reduced to near background levels (Fig. 2a). We also could not observe gliding of microtubules by ZEN-4$^{\Delta N}$ at physiological salt concentrations; ATP perfusion caused release of most microtubules. However, at 25 mM KCl, ATP caused partial release of microtubules (Fig. 2b) and some of the remaining microtubules moved briefly with a velocity similar to that of ZEN-4^{MOT}. These data indicate that the N-terminal extension is critical for motility under physiological ionic conditions. Because microtubules bound to ZEN-4$^{\Delta N}$ in the absence of ATP and dissociated in the presence of ATP, the basic N terminus seems to stabilize the interaction between ZEN-4 and microtubules during the weak binding state when ADP (or ADP + Pi) is bound, analogous to the function of the K-loop in the KIF1A motor[17]. Moreover, in conventional kinesin the N terminus is adjacent to loop 12 (Supplementary Movie 2), the site of the K-loop insertion, which binds to the negatively charged C-terminal tail of tubulin. By analogy, the N terminus of ZEN-4 probably interacts with the C terminus of tubulin.

Because the N-terminal extension has a critical role in the motor activity of ZEN-4, phosphorylation of T9 might regulate this motor. Indeed, phosphorylated ZEN-4^{MOT} had greatly reduced activity in the ATPase assay (Fig. 2c). We also assessed the ability of phosphorylated ZEN-4^{MOT} to support microtubule gliding. Whereas ZEN-4^{MOT} efficiently bound microtubules in the presence of ATP and supported microtubule gliding at high motor density (5×10^4 motors μm^{-2}, 150 mM KCl, average velocity 0.14 $\mu m\,s^{-1}$), after phosphorylation of T9 fewer microtubules remained bound to the surface (Fig. 2d). The remaining microtubules moved with the same average velocity as observed with the unphosphorylated protein, although the gliding was saltatory. At lower motor density (10^4 motors μm^{-2}), unphosphorylated ZEN-4^{MOT} still supported robust motility, but phosphorylated ZEN-4^{MOT} did not bind microtubules

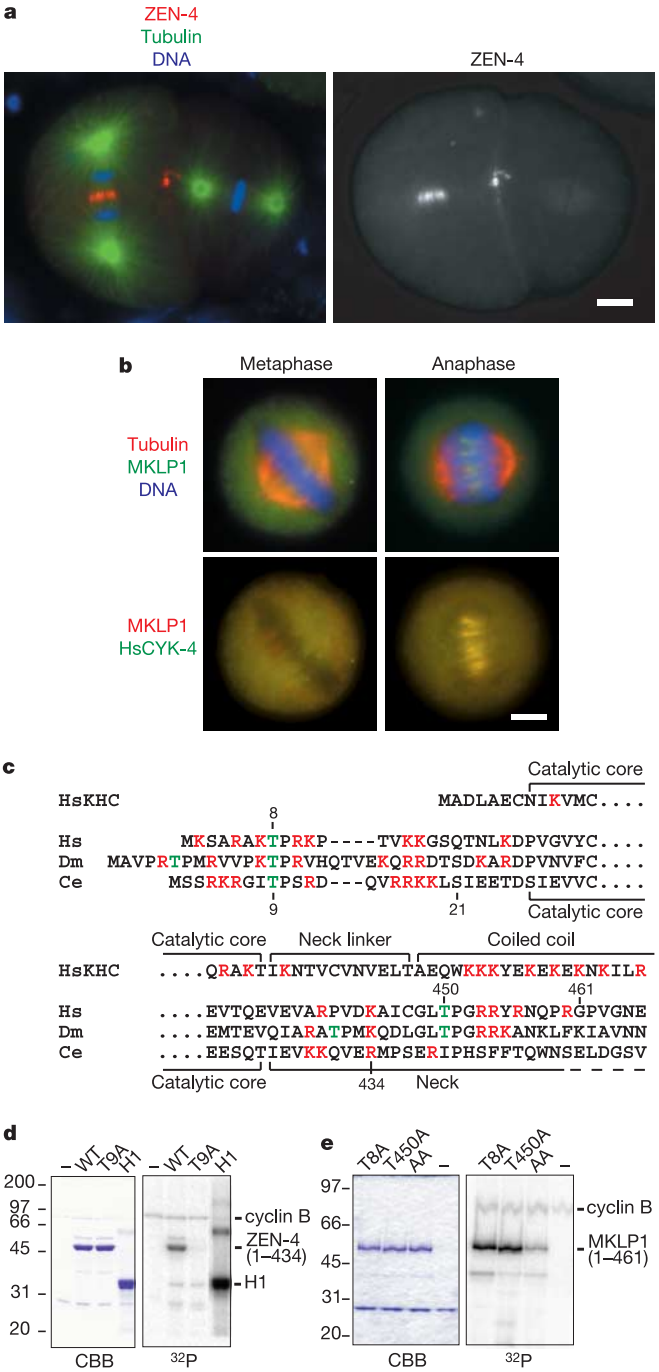

Figure 1 ZEN-4/MKLP1 localizes upon anaphase onset and is a Cdk1 substrate *in vitro*. **a**, **b**, In metaphase, ZEN-4/MKLP1 weakly associates with the spindle and concentrates on the central spindle upon anaphase onset in *C. elegans* embryos (**a**) and HeLa cells (**b**). **c**, ZEN-4/MKLP1 has a conserved consensus site for phosphorylation by Cdk1 N-terminal to the kinesin catalytic core. HsKHC, human kinesin heavy chain; Hs, *Homo sapiens*; Dm, *Drosophila melanogaster*; Ce, *Caenorhabditis elegans*. **d**, ZEN-4^{MOT} is phosphorylated by Cdk1/cyclin B *in vitro*. ZEN-4$^{MOT\text{-}T9A}$ is not phosphorylated (H1, histone H1). WT, wild type. CBB, coomassie blue. **e**, MKLP1 is phosphorylated by Cdk1/cyclin B on T8 and T450. MKLP1 (1–461) mutants T8A, T450A and T8A/T450A, were incubated with Cdk1/cyclin B *in vitro*. Scale bars, 5 μm.

at all (Fig. 2d). We quantified the frequency of microtubules detaching from the surface and found that T9 phosphorylation destabilizes the interaction between ZEN-4^{MOT} and microtubules (Fig. 2e). Cdk1/cyclin B had no effect on ZEN-4$^{MOT\text{-}T9A}$, indicating that these effects were due to phosphorylation of T9 (Fig. 2d, e). Phosphorylation of ZEN-4^{MOT} did not significantly alter the estimated maximum ATPase rate but greatly increased the concentration of microtubules required for maximal activity (Fig. 2f).

Phosphorylation of the ZEN-4 N-terminal extension regulates the biochemical properties of ZEN-4 *in vitro*, therefore we evaluated whether these sites are phosphorylated *in vivo*. Because it is not feasible to obtain mitotic *C. elegans* embryos for biochemical analysis, we investigated the *in vivo* phosphorylation state of the human orthologue MKLP1 by two-dimensional phosphopeptide mapping. The motor domain of MKLP1 contains two Cdk1/cyclin B consensus sites, T8 and T450, that were efficiently phosphorylated by Cdk1/cyclin B (Fig. 1e). Phosphopeptide maps of recombinant MKLP1 motor domain (1–461) with T8A or T450A substitutions revealed one major phosphopeptide in each case, that were used as migration standards (Fig. 3b). HeLa cells were arrested in mitosis, labelled with ^{32}P orthophosphate and MKLP1 was immunopurified. MKLP1 was phosphorylated, as was the coprecipitating HsCYK-4/MgcRacGAP (Fig. 3a). On phosphopeptide maps, MKLP1 from ^{32}P-labelled mitotic cells gave six major phosphopeptides. Two phosphopeptides co-migrated with the phosphoT8 and phosphoT450 standards (Fig. 3b). Thus, both T8 and T450 of MKLP1 are phosphorylated in mitotic cells.

If MKLP1 is delocalized during metaphase as a consequence of phosphorylation by Cdk1/cyclin B, then these sites should be dephosphorylated during anaphase to allow MKLP1 to localize. To evaluate the changes in phosphorylation of the Cdk1/cyclin B sites during the exit from mitosis and the onset of cytokinesis we used an anti-phosphothreonine-proline (TP) antibody on immunoblots of MKLP1 immunoprecipitates. This antibody primarily detects phosphorylation of MKLP1 on T8 and T450 because its reactivity is greatly diminished when these residues are replaced by serines (Fig. 3c). Endogenous MKLP1, immunoprecipitated from nocodazole-arrested cells, was phosphorylated (Fig. 3d; 0 min) and this phosphorylation was stable for ~25 min after release from mitotic arrest, after which time the phosphorylation level was significantly reduced. To show that this phosphorylation is dependent on Cdk1 *in vivo*, mitotic cells were treated with the Cdk1 inhibitor roscovitine[18]. This compound induced rapid dephosphorylation of endogenous MKLP1 on TP sites (Fig. 3e) and caused the protein to concentrate on spindles (Fig. 3f). We conclude that MKLP1 is phosphorylated by Cdk1/cyclin B, and this kinase regulates the localization of MKLP1 *in vivo*.

A candidate phosphatase that could remove this inhibitory

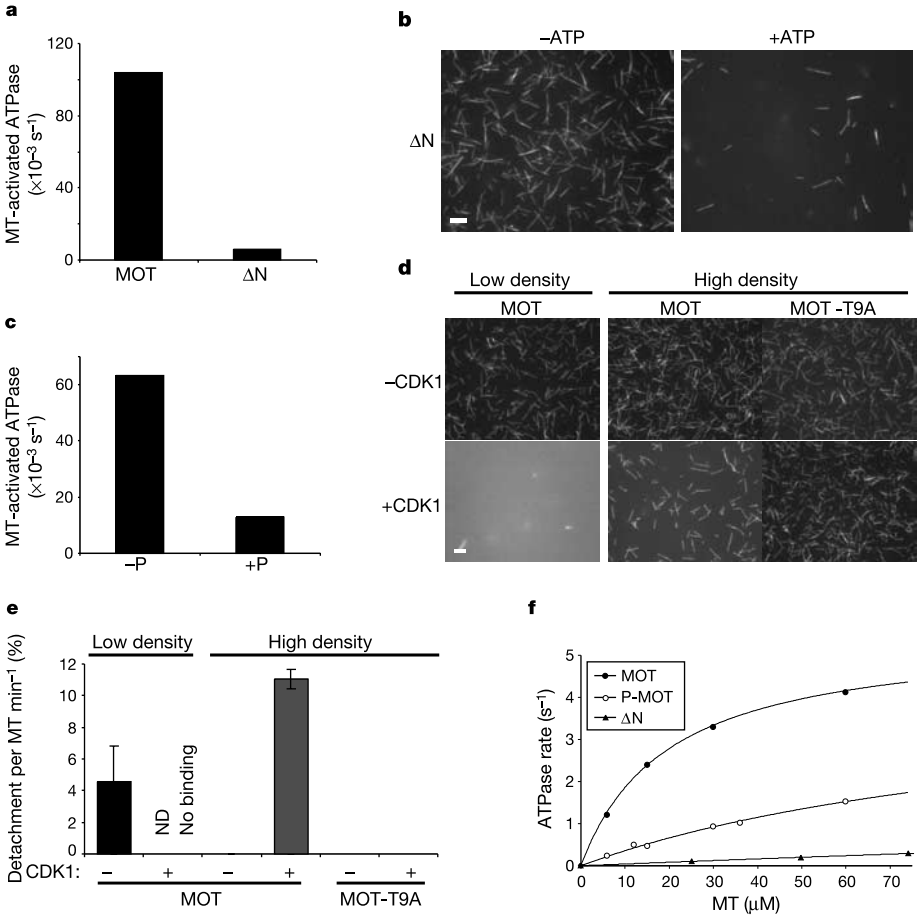

Figure 2 Microtubule (MT) binding by ZEN-4 is inhibited by Cdk1/cyclin B phosphorylation. **a**, ATPase activity of ZEN-4^{MOT} and ZEN-4$^{\Delta N}$. **b**, Microtubule binding by ZEN-4$^{\Delta N}$ in the presence and absence of ATP. **c**, ATPase activity of ZEN-4^{MOT} with (+P) and without (−P) stoichiometric phosphorylation by Cdk1/cyclin B. **d**, Microtubule capture by ZEN-4^{MOT} and ZEN-4 $^{MOT\text{-}T9A}$ in the presence or absence of Cdk1/cyclinB phosphorylation at two densities of ZEN-4. Images shown are frames from a motility assay after ATP addition. **e**, Quantification of the detachment probability (±s.e.m.) at two densities of ZEN-4 as in **d**. **f**, Kinetics of ATP hydrolysis by ZEN-4^{MOT}, phospho-ZEN-4^{MOT} and ZEN-4$^{\Delta N}$ as a function of microtubule concentration. For MOT and P-MOT, the curves shown represent Michaelis–Menten equations with the following constants (maximal ATPase rates (s^{-1}): 5.5, 4.4 and $K_{0.5,MT}$ (μM): 19.6 to 112 for MOT and P-MOT, respectively). Assays shown in **a**–**f** were performed at 150 mM KCl and the assays in **f** were performed at 75 mM KCl. Scale bars, 5 μm

Table 1 **Impaired rescue of *zen-4(w35)* by *zen-4* T9A**

Line	Embryos	Viable adults (%)	Rol animals	Bli animals	Array transmission (%)	Rescue efficiency (%)
zen-4						
1	1,178	46.2	281	66	45.0	49.8
2	789	30.8	101	31	33.0	47.6
3	993	44.1	203	48	39.7	48.7
4	1,491	47.6	355	88	42.9	55.0
5	800	44.9	204	69	46.6	74.1
Total	5,251	43.7	1,144	302	42.3	54.4
zen-4 T9A						
1	1,355	41.3	287	27	48.9	16.3
2	1,157	46.2	270	11	49.5	7.7
3	803	34.1	125	0	45.6	0.0
4	2,010	48.2	361	0	37.3	0.0
Total	5,325	43.8	1,043	38	43.8	6.5

Extrachromosomal transgenic arrays marked by *rol-6*(*su1006*) were generated in *zen-4*(*w35*) *bli-6*(*sc16*)/*unc-44*(*e1260*) *lag-1*(*q385*). Embryos were collected from hermaphrodites and scored for fully developed adults, Rol animals, and Bli animals (all of which were Rol). Rescue efficiency = number of Bli animals/((number of embryos × array transmission *f*)/4), where array transmission *f* = (number of Rol–number of Bli animals)/(number of viable adults–number of Bli animals). No Bli animals were observed in three transgenic lines generated with *rol-6*(*su1006*) and without *zen-4* (>1,000 embryos each). Results shown are the sum of two independent experiments.

phosphorylation and allow MKLP1-dependent central spindle assembly is CDC14. Therefore, we tested whether recombinant human CDC14A could dephosphorylate MKLP1 phosphorylated by Cdk1/cyclin B. Phospho-MKLP1 fragments MKLP1 T8A and MKLP1 T450A, in which T450 and T8 are the major phosphorylation sites, respectively, were dephosphorylated by hCDC14A (Fig. 3g). This phosphatase activity was sensitive to orthovanadate, and human CDC14A with a mutation in the catalytic cysteine (PD) was inactive. *C. elegans* CDC-14 also dephosphorylated ZEN-4 (data not shown). The function of CDC-14 *in vivo* is consistent with it activating ZEN-4 upon anaphase onset.

Phosphorylation of ZEN-4 at T9 significantly affects its motor activity *in vitro* and the corresponding site is phosphorylated in human cells. To determine whether this phosphorylation is essential *in vivo*, we generated a *C. elegans* strain containing a null allele (*w35*) of ZEN-4 linked to a recessive visible marker, *bli-6*, which causes cuticle blistering. The *w35* allele causes embryonic lethality[10]; this lethality is associated with cytokinesis defects in embryos at the 100–300-cell stage (Fig. 4a). We generated multiple independent transgenic lines expressing either ZEN-4 or ZEN-4 T9A. Whereas wild-type ZEN-4 could effectively rescue *zen-4(w35)*, the T9A substitution reduced the rescue efficiency ~8-fold (Table 1). Thus, ZEN-4 with a non-phosphorylatable residue at position 9 is defective *in vivo*.

To determine whether the phosphorylation of MKLP1 on T8 and T450 regulates its localization in human cells, we expressed Myc-tagged wild-type and mutant proteins (where T8 and T450 were mutated to alanine; MKLP1-AA) in HeLa cells. Although ectopically expressed wild-type protein localized on metaphase spindles to a greater extent than the endogenous protein, MKLP1-AA was significantly more enriched on the spindle (Fig. 4b), suggesting that phosphorylation regulates MKLP1 localization.

Phosphorylation of MKLP1 during metaphase may ensure that central spindle assembly does not occur before anaphase onset. For example, if kinetochore microtubules become bundled to antiparallel microtubules from the opposite spindle pole during metaphase, efficient segregation of chromosomes during anaphase could be impaired. To test this hypothesis, synchronized HeLa cells expressing MKLP1 or MKLP1-AA were fixed at anaphase and the frequency of aberrant chromosome segregation was assessed. An increase in chromosome bridges was observed with both MKLP1 derivatives. However, the frequency of lagging chromosomes was significantly higher when cells expressed MKLP1-AA compared with MKLP1 (Fig. 4c, d). Therefore, phosphorylation of MKLP1 during metaphase inhibits its association with the spindle and prevents the induction of aneuploidy.

To determine whether CDC-14 is the critical phosphatase that

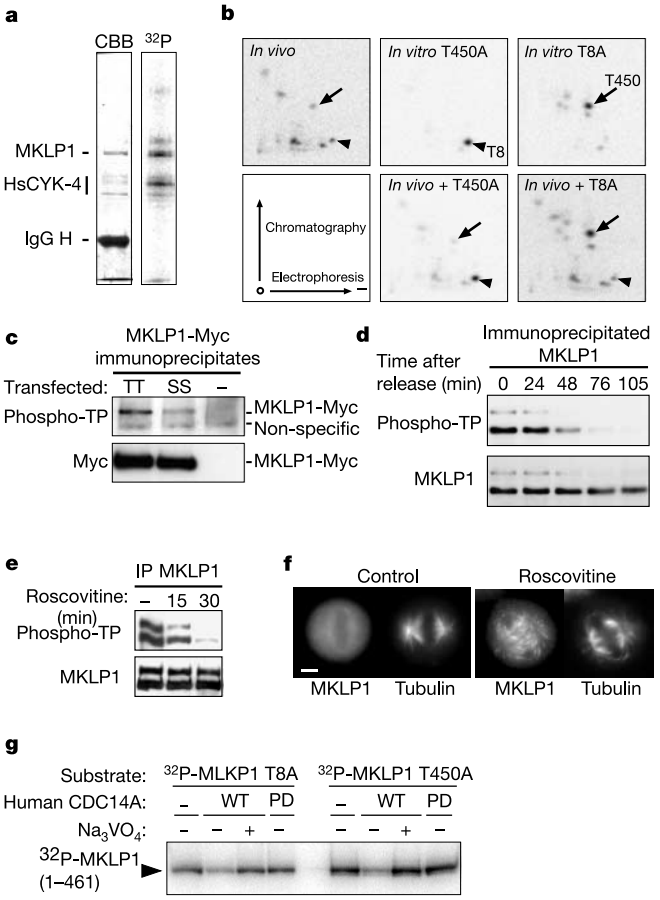

Figure 3 MKLP1 is phosphorylated on Cdk1/cyclin B sites in metaphase and dephosphorylated during anaphase. **a**, Immunoprecipitation of centralspindlin from metabolically labelled mitotic HeLa cells. **b**, Two-dimensional peptide maps of phosphoMKLP1 and *in vitro* generated phosphoMKLP1 T450A and phosphoMKLP1 T8A. **c**, Immunoprecipitates of MKLP1-Myc (TT) and MKLP1 T8ST450S-Myc (SS) were immunoblotted with a phosphoTP antibody revealing that this antibody primarily reacts with phosphoT8 and phosphoT450. **d**, Immunoblot with phosphoTP antibody of MKLP1 immunoprecipitated from cells released from a nocodazole block for the indicated times. **e**, Immunoblot with phosphoTP antibody of MKLP1 immunoprecipitated from cells arrested in mitosis with nocodazole and treated with roscovitine for the indicated times. **f**, Localization of MKLP1 and tubulin in cells treated as in **e**, except that 20 ng ml^{-1} nocodazole was used to induce arrest. **g**, Dephosphorylation of phosphoMKLP1 T450A and phosphoMKLP1 T8A by human CDC14A (WT) *in vitro*. Mutation of the catalytic cysteine 278 to serine (PD) or addition of sodium vanadate renders the enzyme inactive. Scale bars, 5 μm.

dephosphorylates T9, we investigated whether, unlike wild-type ZEN-4, the T9A mutant can localize during anaphase in embryos depleted of CDC-14. *C. elegans* strains, expressing ZEN-4::GFP (green fluorescent protein) or ZEN-4::GFP T9A in the germline, were generated. CDC-14 was depleted by RNAi and the behaviour of ZEN-4::GFP was monitored by time-lapse microscopy. ZEN-4::GFP rarely localized to the central spindle when CDC-14 was depleted (3 of 19 embryos), as shown previously[12]. In contrast, the non-phosphorylatable mutant ZEN-4::GFP T9A localized in nearly all *cdc-14*(*RNAi*) embryos (20 of 22 embryos) (Fig. 4e). We conclude that localization of ZEN-4::GFP T9A requires less CDC-14 activity than does localization of ZEN-4::GFP. As a control, we found that strains expressing wild-type or T9A derivatives of ZEN-4::GFP were equally sensitive to *rhoA*(*RNAi*) and *let-21*(*RNAi*) (Fig. 4e and data not shown). Thus, dephosphorylation of phospho-T9 is CDC-14-dependent *in vivo* and may well be direct. Lines expressing ZEN-4 T9A segregated males at elevated frequency compared with lines expressing the wild-type protein (ZEN-4, 0.16%, $n = 3{,}703$; ZEN-4::T9A, 0.55%, $n = 4{,}883$). In *C. elegans*, males arise at low frequency owing to non-disjunction of the X chromosome in the hermaphrodite germ line, hence these data provide further evidence that failure to phosphorylate this site induces defects in chromosome segregation.

We have shown that ZEN-4/CeMKLP1 has microtubule motility *in vitro*. Motor activity seems to be essential *in vivo* as well, because mutations in the ATP-binding P-loop prevent discrete localization of MKLP1 to the central spindle and prevent normal central spindle assembly and completion of cytokinesis[19,20]. Microtubule binding by MKLP1 involves a highly basic N-terminal extension of the motor, which may interact with the C-terminal acidic tail of tubulin in a manner similar to the K-loop in KIF1A (ref. 21). The function of this basic region is regulated by direct phosphorylation by Cdk1/cyclin B *in vitro*, and the equivalent site in MKLP1 was shown to be phosphorylated *in vivo*. Basic clusters are present in the N terminus of numerous kinesin-like proteins, and many of these clusters contain, or are adjacent to, phosphoacceptor sites. The microtubule depolymerizing activity of MCAK has been shown to be inhibited by Aurora B phosphorylation of a serine residue within a region rich in basic residues[22–24]. Phosphorylation of residues embedded in basic stretches that may interact with the C-terminal acidic tail of tubulin might therefore be a general mechanism to regulate kinesin-like proteins.

ZEN-4 mediates central spindle assembly by bundling the plus ends of antiparallel microtubules. This activity may need to be inhibited during metaphase to prevent bundling of a kinetochore fibre to microtubules nucleated by the other spindle pole. In budding yeast, Cdk1/cyclin B and Cdc14p antagonistically control the localization of Aurora B–Incenp (inner centromere protein complex) and chromosome segregation defects result from the precocious localization of this complex[5]. PRC1, a microtubule binding protein important for central spindle assembly, is inhibited by phosphorylation on Cdk1/cyclin B consensus sites[25]. Thus, during metaphase, multiple mechanisms prevent microtubule bundling and thereby maintain a stable karyotype. □

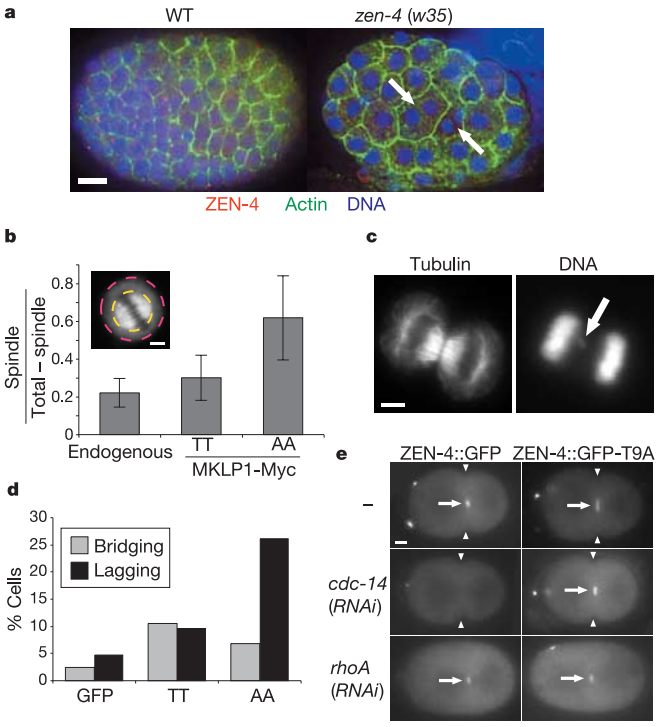

Figure 4 Non-phosphorylatable MKLP1 induces lagging chromosomes, and non-phosphorylatable ZEN-4 localizes in embryos depleted of CDC-14. **a**, *zen-4*(*w35*) embryos are cytokinesis-defective during early embryogenesis (arrows, binucleate cells) (ZEN-4, red; DNA, blue; actin, green). Homozygous mutant embryos were identified by a strong reduction in the ZEN-4 staining at equivalent stages and this was always associated with multinucleated blastomeres. **b**, Quantification of the spindle localization of MKLP1-Myc, MKLP1-AA-Myc and endogenous MKLP1. The ratio (±s.d.) of the spindle fluorescence to non-spindle fluorescence was calculated as described in the methods. The inset shows MKLP1AA-Myc concentrates on the metaphase spindle in HeLa cells. Circles indicate regions used for the quantification of the extent of spindle localization. **c**, Overexpression of MKLP1-AA causes lagging chromosomes (arrow). **d**, Quantification of the frequency of anaphase bridging and lagging chromosomes in cells transfected with MKLP1 ($n = 105$ cells), MKLP1-AA ($n = 109$) or GFP ($n = 84$). **e**, ZEN-4 T9A, but not ZEN-4, can localize in *cdc-14*(*RNAi*) embryos (arrows), whereas both strains were equally susceptible to *rhoA*(*RNAi*) as evidenced by the absence of cleavage furrow ingression (arrowheads). Scale bars, 5 μm.

Methods

Nematode strains and alleles

The following strains and alleles were used: EH135 (*unc-44*(*e362*) *bli-6*(*sc16*) *IV*), SU62 (*unc-44*(*e1260*) *lag-1*(*q385*)/*zen-4*(*w35*) *IV*), MG376 (*zen-4*(*w35*) *bli-6*(*sc16*)/*unc-44*(*e1260*) *lag-1*(*q385*)). Some strains used in this study were provided by the *Caenorhabditis* Genetics Center, which is funded by the NIH NCRR. For rescue assays, simple transgene arrays were prepared as described[26] using pRF4 at 80 ng μl^{-1}, and MP66 (*zen-4*) and MM196 (*zen-4 T9A*) at 10 ng μl^{-1}. To analyse ZEN-4::GFP localization in the early embryo, complex arrays that rescue *zen-4*(*or153*ts) were prepared as described[27]. Depletion of CDC-14 by RNAi was performed as described[12], using dsRNA corresponding to nucleotides 51–1214 of C17G10.4C.

Cell culture and transfection

HeLa cells were cultured in DMEM with fetal bovine serum. MKLP1 derivatives, containing a C-terminal triple Myc tag, were transfected using LipofectAmine PLUS (Invitrogen). To analyse chromosome segregation defects, cells were synchronized with a double thymidine block and transfected with Fugene 6 (Roche) 23 h before release from the second block. Eleven hours after release of the block, mitotic cells were collected by shake-off, and re-plated and fixed 30 min later. For inhibitor experiments, cells were synchronized in mitosis with 40 ng ml^{-1} nocodazole, then 100 μM roscovitine (Calbiochem) was added for the indicated times before analysis.

Protein preparation

For kinase assays, ZEN-4 and MKLP1 motor domains were cloned into pCBD-TEV and expressed in bacteria as fusion proteins with chitin-binding domain at the N terminus[3]. For gliding assays these constructs were modified to include a C-terminal flexible linker and biotin-acceptor sequence (GTGSG-GLNDIFEAQKIEWHE) (ref. 28). Recombinant proteins were affinity-purified with chitin beads and eluted with TEV (tobacco etch virus) protease. All the proteins except those used in Fig. 1d were further purified by ion exchange chromatography (MonoS for ZEN-4^{MOT} (1–434) and MKLP1 constructs, and MonoQ for ZEN-4$^{\Delta N}$ (21–434)) followed by gel filtration (Superdex 200, Pharmacia) chromatography. Human CDC14A was amplified from human testis complementary DNA and cloned into pGEX-5X-1. Phosphatase-dead human CDC14A was generated by mutating cysteine 278 to serine. The resulting GST fusion proteins were expressed and purified according to standard procedures.

Kinase and phosphatase assays

For kinase assays, 0.1–0.2 mg ml^{-1} ZEN-4 and MKLP1 proteins were incubated with purified recombinant human Cdk1/GST–cyclin B in kinase buffer (50 mM KCl, 2 mM

MgCl2, 1 mM EGTA, 10 mM PIPES (pH 6.8), 1 mM DTT, 50 μM ATP and 50 μCi ml^{-1} [ϒ-^{32}P]ATP) at 25 °C (ref. 29). To prepare substrates for the phosphatase assay, free radiolabelled ATP was removed by repeated dilution and concentration with microcon-30 filtration devices. For phosphatase assays, 0.6 mg ml^{-1} phospho-MKLP1 was incubated with 60 μg ml^{-1} bacterially expressed recombinant GST–human CDC14A in phosphatase buffer (50 mM KCl, 1 mM $MgCl_2$, 1 mM EGTA, 1 mM DTT and 10 mM PIPES (pH 6.8)) at 25 °C.

ATPase and microtubule motility assays

For the ATPase assay in Fig. 2b, phosphorylated ZEN-4 motor domain was purified from unphosphorylated ZEN-4 by Mono S and Superdex 200 (Pharmacia) chromatography. The control unphosphorylated sample was also re-purified with these columns. ZEN-4 motor domains were incubated with 5 μM taxol-stabilized microtubules from phosphocellulose-purified bovine brain tubulin in ATPase buffer (150 mM KCl, 10 mM PIPES (pH 6.8), 2 mM MgCl2, 1 mM EGTA, 2 mM ATP, 1 mM DTT and 5 μM taxol) at 25 °C. In Fig. 2f, 75 mM KCl was used in the ATPase buffer. Free phosphate release was measured by colorimetry with molybdate/malachite green. For surface binding and gliding assays, bacterially biotinylated ZEN-4 motor domains were immobilized on a coverslip sequentially coated with biotin-BSA and NeutrAvidin (Molecular Probes)[16]. The extent of biotinylation was estimated by western blotting with an anti-biotin antibody (Sigma).

Analysis of *in vivo* phosphorylation state

For mitotic synchronization, cells were arrested for 14 h with 2.5 mM thymidine. The cells were released for 7.5 h and then 50 ng ml^{-1} nocodazole was added for 3.5 h to establish an M-phase arrest. For phosphopeptide mapping, 0.3 mCi ml^{-1} ^{32}P-orthophosphate was added with the nocodazole. Lysates were prepared with IP buffer (150 mM NaCl, 10 mM NaF, 40 mM β-glycerophosphate, 20 mM HEPES (pH 7.5), 2 mM $MgCl_2$, 10 mM EDTA, 0.5% Triton X-100, 1 mM DTT, 1 mM PMSF, 50 μg ml^{-1} leupeptin, 50 μg ml^{-1} pepstatin and 1 μM microcystin). MKLP1 was immunoprecipitated with anti-MKLP1 antibody bound to protein-A Sephadex beads and resolved by SDS–polyacrylamide gel electrophoresis. Phosphoproteins were digested in-gel with trypsin. Eluted peptides were analysed using pH 1.9 electrophoresis buffer[30]. Phosphorylation at TP sites was detected with an anti-phosphoTP monoclonal antibody (Cell Signalling Technology).

Immunolocalization and microscopy

HeLa cells were fixed with −20 °C methanol and stained as described before. To detect the Myc-epitope, an affinity purified rabbit antiserum (Gramsch Laboratories) was used. To estimate the accumulation of Myc-tagged MKLP1, the area of the cell (a_T) and of the spindle region (a_S), and the mean intensity of the cell (m_T) and of the spindle region (m_S) were measured from unprocessed 12-bit images with ImageJ (http://rsb.info.nih.gov/ij/). The ratio between spindle-derived signal and the non-spindle-derived signal was calculated as $(m_S - m_T)(a_S/(m_T a_T - m_S a_S))$. Images were collected on either a Zeiss Axioplan II imaging microscope fitted with a CoolSnap Fx CCD camera or a DeltaVision Imaging System (Applied Precision).

Received 27 April; accepted 16 June 2004; doi:10.1038/nature02767.
Published online 28 July 2004.

1. Scholey, J. M., Brust-Mascher, I. & Mogilner, A. Cell division. *Nature* **422,** 746–752 (2003).
2. Glotzer, M. Animal cell cytokinesis. *Annu. Rev. Cell Dev. Biol.* **17,** 351–386 (2001).
3. Mishima, M., Kaitna, S. & Glotzer, M. Central spindle assembly and cytokinesis require a kinesin-like protein/RhoGAP complex with microtubule bundling activity. *Dev. Cell* **2,** 41–54 (2002).
4. Adams, R. R., Carmena, M. & Earnshaw, W. C. Chromosomal passengers and the (aurora) ABCs of mitosis. *Trends Cell Biol.* **11,** 49–54 (2001).
5. Pereira, G. & Schiebel, E. Separase regulates INCENP-Aurora B anaphase spindle function through Cdc14. *Science* **302,** 2120–2124 (2003).
6. Romano, A. *et al.* CSC-1: A subunit of the Aurora B kinase complex that binds to the Survivin-like protein BIR-1 and the Incenp-like protein ICP-1. *J. Cell Biol.* **161,** 229–236 (2003).
7. Sellitto, C. & Kuriyama, R. Distribution of a matrix component of the midbody during the cell cycle in Chinese hamster ovary cells. *J. Cell Biol.* **106,** 431–439 (1988).
8. Jantsch-Plunger, V. *et al.* CYK-4: A Rho family GTPase activating protein (GAP) required for central spindle formation and cytokinesis. *J. Cell Biol.* **149,** 1391–1404 (2000).
9. Powers, J., Bossinger, O., Rose, D., Strome, S. & Saxton, W. A nematode kinesin required for cleavage furrow advancement. *Curr. Biol.* **8,** 1133–1136 (1998).
10. Raich, W. B., Moran, A. N., Rothman, J. H. & Hardin, J. Cytokinesis and midzone microtubule organization in *Caenorhabditis elegans* require the kinesin-like protein ZEN-4. *Mol. Biol. Cell* **9,** 2037–2049 (1998).
11. Gray, C. H., Good, V. M., Tonks, N. K. & Barford, D. The structure of the cell cycle protein Cdc14 reveals a proline-directed protein phosphatase. *EMBO J.* **22,** 3524–3535 (2003).
12. Gruneberg, U., Glotzer, M., Gartner, A. & Nigg, E. A. The CeCDC-14 phosphatase is required for cytokinesis in the *Caenorhabditis elegans* embryo. *J. Cell Biol.* **158,** 901–914 (2002).
13. Parry, D. H. & O'Farrell, P. H. The schedule of destruction of three mitotic cyclins can dictate the timing of events during exit from mitosis. *Curr. Biol.* **11,** 671–683 (2001).
14. Wheatley, S. P. *et al.* CDK1 inactivation regulates anaphase spindle dynamics and cytokinesis *in vivo*. *J. Cell Biol.* **138,** 385–393 (1997).
15. Nislow, C., Lombillo, V. A., Kuriyama, R. & McIntosh, J. R. A plus-end-directed motor enzyme that moves antiparallel microtubules *in vitro* localizes to the interzone of mitotic spindles. *Nature* **359,** 543–547 (1992).
16. Berliner, E. *et al.* Microtubule movement by a biotinated kinesin bound to streptavidin-coated surface. *J. Biol. Chem.* **269,** 8610–8615 (1994).
17. Okada, Y. & Hirokawa, N. Mechanism of the single-headed processivity: diffusional anchoring between the K-loop of kinesin and the C terminus of tubulin. *Proc. Natl Acad. Sci. USA* **97,** 640–645 (2000).
18. Meijer, L. *et al.* Biochemical and cellular effects of roscovitine, a potent and selective inhibitor of the cyclin-dependent kinases cdc2, cdk2 and cdk5. *Eur. J. Biochem.* **243,** 527–536 (1997).
19. Matuliene, J. & Kuriyama, R. Kinesin-like protein CHO1 is required for the formation of midbody matrix and the completion of cytokinesis in mammalian cells. *Mol. Biol. Cell* **13,** 1832–1845 (2002).
20. Minestrini, G., Harley, A. S. & Glover, D. M. Localization of Pavarotti-KLP in living *Drosophila* embryos suggests roles in reorganizing the cortical cytoskeleton during the mitotic cycle. *Mol. Biol. Cell* **14,** 4028–4038 (2003).
21. Kikkawa, M. *et al.* Switch-based mechanism of kinesin motors. *Nature* **411,** 439–445 (2001).
22. Andrews, P. D. *et al.* Aurora B regulates MCAK at the mitotic centromere. *Dev. Cell* **6,** 253–268 (2004).
23. Lan, W. *et al.* Aurora B phosphorylates centromeric MCAK and regulates its localization and microtubule depolymerization activity. *Curr. Biol.* **14,** 273–286 (2004).
24. Ohi, R., Sapra, T., Howard, J. & Mitchison, T. J. Differentiation of cytoplasmic and meiotic spindle assembly MCAK functions by Aurora B-dependent phosphorylation. *Mol. Biol. Cell* **15,** 2895–2906 (2004).
25. Mollinari, C. *et al.* PRC1 is a microtubule binding and bundling protein essential to maintain the mitotic spindle midzone. *J. Cell Biol.* **157,** 1175–1186 (2002).
26. Mello, C. & Fire, A. DNA transformation. *Methods Cell Biol.* **48,** 451–482 (1995).
27. Kaitna, S., Mendoza, M., Jantsch-Plunger, V. & Glotzer, M. Incenp and an aurora-like kinase form a complex essential for chromosome segregation and efficient completion of cytokinesis. *Curr. Biol.* **10,** 1172–1181 (2000).
28. Beckett, D., Kovaleva, E. & Schatz, P. J. A minimal peptide substrate in biotin holoenzyme synthetase-catalyzed biotinylation. *Protein Sci.* **8,** 921–929 (1999).
29. Patra, D. & Dunphy, W. G. Xe-p9, a *Xenopus* Suc1/Cks protein, is essential for the Cdc2-dependent phosphorylation of the anaphase-promoting complex at mitosis. *Genes Dev.* **12,** 2549–2559 (1998).
30. Boyle, W. J., van der Geer, P. & Hunter, T. Phosphopeptide mapping and phosphoamino acid analysis by two-dimensional separation on thin-layer cellulose plates. *Methods Enzymol.* **201,** 110–149 (1991).

Supplementary Information accompanies the paper on **www.nature.com/nature**.

Acknowledgements This work was supported by a grant from the Austrian Science Foundation and with the support of Boehringer Ingelheim. M.M., V.P. and M.G. would like to thank K. Bartalska for technical assistance, and S. Kaitna and K. Mechtler for help in the initial stages of this project.

Competing interests statement The authors declare that they have no competing financial interests.

Correspondence and requests for materials should be addressed to M.G. (mglotzer@imp.univie.ac.at).

Structural basis for inhibition of the replication licensing factor Cdt1 by geminin

Changwook Lee[1], BumSoo Hong[1]*, Jung Min Choi[1]*, Yugene Kim[1], Saori Watanabe[2], Yukio Ishimi[3], Takemi Enomoto[2], Shusuke Tada[2], Youngchang Kim[4] & Yunje Cho[1]

[1]*National Creative Research Center for Structural Biology and Department of Life Science, Pohang University of Science and Technology, Hyo-ja dong, San31, Pohang, KyungBook, South Korea*
[2]*Graduate School of Pharmaceutical Sciences, Tohoku University, Aoba-Ku, Senda, Miyagi 980-8578, Japan*
[3]*Biomolecular and Technology Department, Mitsubishi Kagaku Institute of Life Sciences, 11 Minamiooya, Machida, Tokyo 194-8511, Japan*
[4]*Bioscience Division, Structural Biology Center, Argonne National Laboratory, 9700 South Cass Avenue, Argonne, Illinois 60439, USA*

* These authors contributed equally to the work.

To maintain chromosome stability in eukaryotic cells, replication origins must be licensed by loading mini-chromosome maintenance (MCM2–7) complexes once and only once per cell cycle[1–9]. This licensing control is achieved through the activities of geminin[10–12] and cyclin-dependent kinases[9,13,14]. Geminin binds tightly to Cdt1, an essential component of the replication licensing system[6,15–18], and prevents the inappropriate reinitiation of replication on an already fired origin. The inhibitory effect of geminin is thought to prevent the interaction between Cdt1 and the MCM helicase[19,20]. Here we describe the crystal structure of the mouse geminin–Cdt1 complex using tGeminin (residues 79–157, truncated geminin) and tCdt1 (residues 172–368, truncated